Vol. 86 No. 5 pp. 1200–1210 ACTA GEOLOGICA SINICA (English Edition) Oct. 2012

Geochemistry of Carboniferous Sandstones (Sardar Formation), East-Central Iran: Implication for Provenance and Tectonic Setting

Mohammad KHANEHBAD*, Reza MOUSSAVI-HARAMI, Asadollah MAHBOUBI, Mehdi NADJAFI and Mohammad Hosein MAHMUDY GHARAIE

Department of Geology, Faculty of Sciences, Ferdowsi University of Mashhad, Mashhad, Iran

Abstract: Geochemical analysis of sandstones from the Sardar Formation (from two stratigraphic successions) in east-central Iran were used for identification of geochemical characterization of sandstones, provenance and tectonic setting. Sandstones in the two lithostratigraphic successions have similar chemical compositions suggesting a common provenance. Bulk-rock geochemistry analysis of Carboniferous sandstones from Sardar Formation indicates that they are mainly quartz dominated and are classified as quartzarenites, sublitharenites and subarkoses, derived from acid igneous to intermediate igneous rocks. Discrimination function analysis indicates that the sandstones of Sardar Formation were derived from quartzose sedimentary provenance in a recycled orogenic setting. Also, major and trace elements in sandstones of Sardar Formation (e.g., K_2O/Na_2O vs. SiO_2) indicate deposition in a stable passive continental margin (PM). Chemical index of alteration (CIA) for these rocks (> 65%) suggests a moderate to relatively high degree of weathering in the source area.

Key words: provenance, Carboniferous, tectonic setting, geochemistry, Sardar Formation, Iran

1 Introduction

Provenance analysis can be used to identify predepositional history of sedimentary rocks. The chemical composition of sedimentary rocks is mostly controlled by source rocks. The analysis of major and trace elements reveal details of sediment composition and tectonic setting of the sedimentary basin. The geochemical composition of detritus rocks is a function of complex verities such as provenance, weathering, transportation and diagenetic processes (Bhatia, 1983). Bhatia (1983) indicated that the ratio of Al_2O_3/SiO_2 gives an indication of the quartz enrichment in sandstones. The ratio K_2O/Na_2O is a measure of the potassium feldspar and mica versus plagioclase content in sandstones. Roser and Korsch (1986) used the ratio of K_2O/Na_2O and SiO_2 content of published data from ancient sedimentary suites to define different tectonic settings such as passive margin (PM), active continental margin (ACM) and oceanic island arc (ARC). Roser and Korsch (1998), for sandstones and argillites of selected New Zealand terranes, used discriminate function analysis elements (TiO_2, Al_2O_3, total Fe_2O_3, MgO, CaO, Na_2O and K_2O) in discriminating four different provenance groups: (1) mafic, (2) intermediate-dominantly andesitic detritus, (3) felsic and plutonic and volcanic detritus and (4) recycled mature polycyclic quartzose detritus. The purpose of this study is to interpret the provenance, tectonic setting and weathering conditions of source rocks of the Carboniferous sandstones of Sardar Formation (Fig. 1) based on petrography and geochemical analysis. Petrography, major and trace elements of 30 sandstone samples from Carboniferous Sardar Formation, east central Iran, have been examined to reach the goal of this study. Interpretation of provenance and tectonic setting of the Carboniferous, based on the Sardar Formation sandstones, are important because it can help in better understanding the paleogeographic reconstruction during this period in a remote area of Central Iran as well as in the Middle East.

2 Geological Setting

The Paleozoic succession of east central Iran was deposited in north-south trending Tabas Block, which was bound by the Kalmard-Kuhbanan right-lateral strike slip fault in the west and the Nayband right-lateral strike slip fault in the east (Alavi, 1996). Central Iran, along with the Alborz Mountains of northern Iran, is located between the Neotethys and Paleotethys sutures of Iran and it is part of

* Corresponding author. E-mail: mkhanehbad@ferdowsi.um.ac.ir

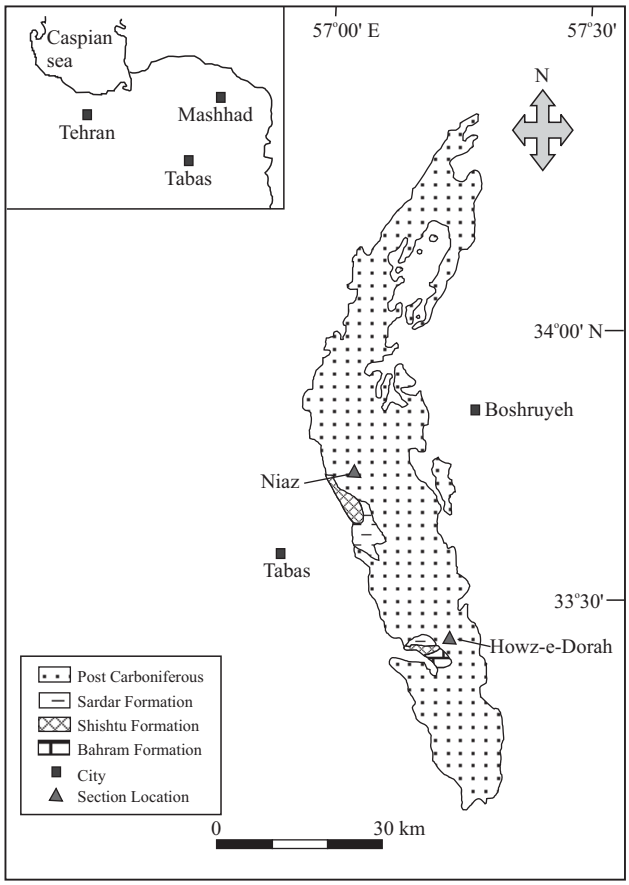

Fig. 1. Simplified geologic map of the study area.

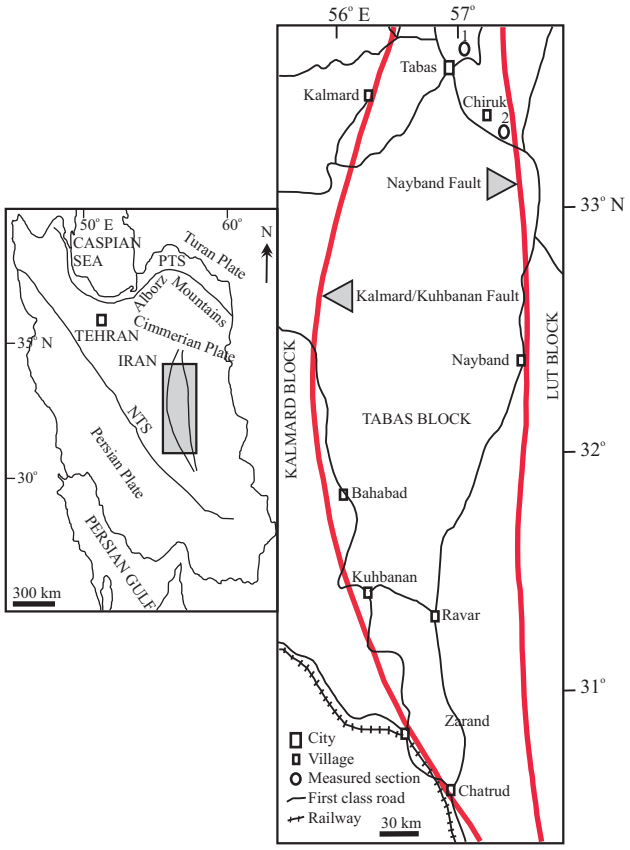

Fig. 2. Location map of the Tabas Block (between the Kalmard-Kuhbanan fault in the west and the Nayband fault in the east) in East Central Iran (1: Niaz section, 2: Howz-e-Dorah section). The area between the Paleotethys suture (PTS) and Neotethys suture (NTS) on the index map comprises the Cimmerian plates of central and northern Iran (modified after Lasemi et al., 2008).

the Cimmerian Continent of Sengor (1984), which was separated from the Gondwana super-continent during the Permian time (e.g., Dercourt et al., 1993; Stampfli and Pillevuit, 1993; Scotese and Langford, 1995; Lasemi, 2001). The Tabas Block is part of the Cimmerian continent with an area of approximately 50 000 km^2 (Lasemi et al., 2008). Based on regional facies and sequence stratigraphic analyses of the Paleozoic deposits of Iran (Lasemi, 2001), the Tabas Block is considered as a failed rift basin, related to the Paleotethys margin during Devonian to Late Triassic time which was separated, along with the rest of the Cimmerian Plate, from northern Gondwana during the Permian. The Sardar Formation (Carboniferous) crops out along the bounding faults of the Tabas Block and is distinguished by its characteristic siliciclastic facies in the field (Fig. 2). The Sardar Formation occurs in two disconnected large outcrops, one at the west foot of Kuh-e-Shotori across the Sardar valley (Niaz section with 656 m thickness), and the other at the south-foot of Kuh-e-Jamal (Howz-e-Dorah section with 584 m thickness). The type section (Niaz section) is not an ideal section, because the lowermost part of the formation and its contact with older rocks is not exposed. However, the Howz-e-Dorah section is introduced as a reference section in this study, in order to illustrate the contact relations with the underlying rocks. The Sardar Formation unconformably overlies member 2 of the Shishtu Formation (early Carboniferous), which is about 220 m thick and consists mainly of gray, thin to intermediate bedded limestone and is unconformably overlain by Permian Jamal Formation, which is over 500 m thick and consists of thick bedded to massive limestone and dolomite. The sedimentary succession of the Sardar Formation consists of alternating sandstones, shales and limestones. Sandstones are mainly quartzarenites, sublitharenites and subarkoses. These framework components are diagnostic of a quartzose recycled orogen provenance (Dickinson et al., 1983; Dickinson, 1985).

3 Materials and Methods

Two stratigraphic sections (at Niaz and Howz-e-Dorah localities) were measured, described and sampled in the field (Fig. 3). A total 285 samples were collected and thin sections were made from these samples for petrographic analysis. The major and trace element concentrations of 30

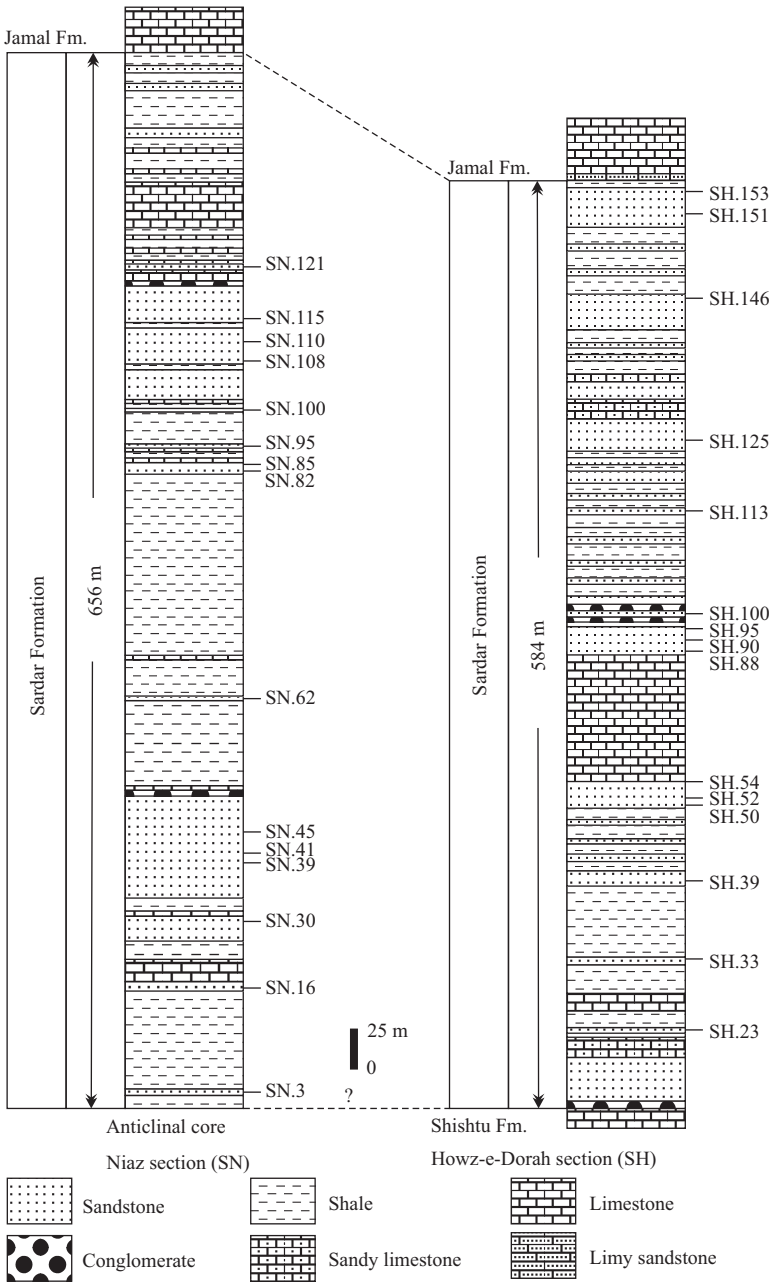

Fig. 3. Columnar sections of the Sardar Formation, showing sample locations.

samples were determined by X-ray fluorescence spectrometer (XRF) at Spectrum Kansaran Binaloud (Mine Material Research Co.), Mashhad, Iran (Philips PW 1480 X-ray spectrometer).

4 Results and Discussion

4.1 Sandstone petrography

The Sardar Formation sandstone is medium to fine grained and are quartz rich (Fig. 4a), associated with slightly lithic grains (sedimentary rock fragments), feldspar and mica. Quartz is the dominant framework grains that consist of nearly 90% of the rock volume and occurring as monocrystalline with a few polycrystalline grains (Fig. 4b). Monocrystalline quartz grains are mainly exhibiting unit extinction. The dominance of monocrystalline quartz grains indicate that the sediments may have been derived from a granitic source (Basu et al., 1975). Calcite and dolomite are found both as detritus grains and cements (Fig. 4c). The heavy mineral assemblage includes rounded tourmaline, zircon and opaque minerals (Fig. 4d). Zircon and tourmaline contents reflect that they may have released from acidic plutonic rocks. As stated above, the quartz grains are generally medium grained, moderately to well sorted, sub angular and sub rounded and show straight to concavo-convex grain contact (Fig. 4e). Hematite is also

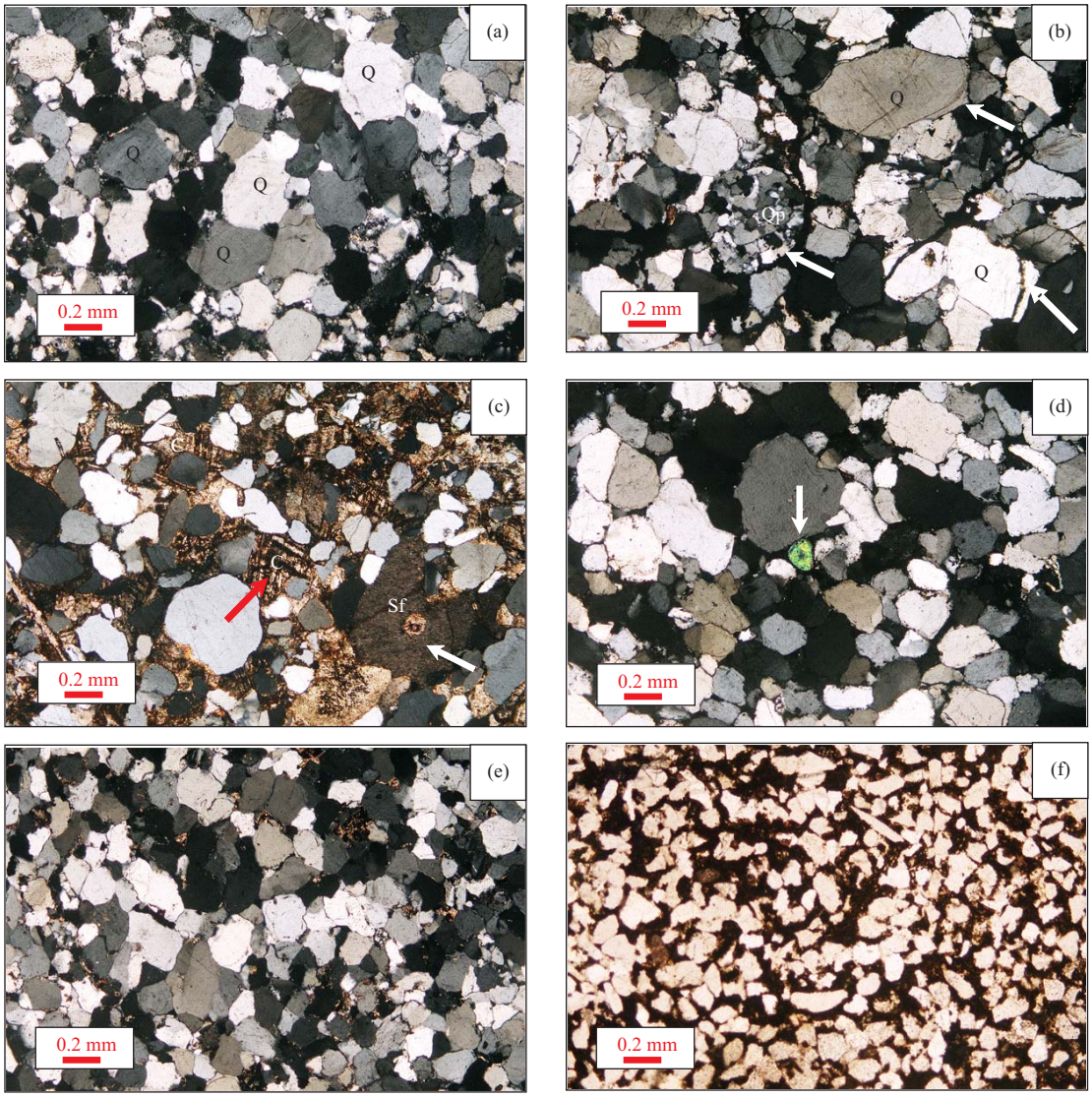

Fig. 4. Sandstones of Sardar Formation.
a, quartz (Q) rich and bimodality in quartzarenite, XPL; b, overgrowth and polycrystalline quartz (Qp) in quartzarenite, XPL; c, carbonate (C) as cement and skeletal fragment (Sf) in sandstone, XPL; d, tourmaline on center in quartzarenite, XPL; e, straight, concavo-convex and suture contact in sandstone, XPL; f, hematitic cement in sandstone, PPL

found as cements (Fig. 4f).

4.2 Chemical composition

The major and trace elemental results of the sandstones from Sardar Formation are presented in Table 1.

4.2.1 Major elements oxides

Sandstones at the Niaz section have high SiO_2 content (73–96%, on average 85%), but other oxides such as TiO_2 with average (1.5%), Al_2O_3 (7%), and Fe_2O_3+MgO around 2% are relatively low. At the Howz-e-Dorah section, sandstones have high SiO_2 content (72–98%, on average 86%), but TiO_2, Al_2O_3 and Fe_2O_3+MgO are 0.27%, 5% and 2%, respectively. The source of silica is mainly quartz, chert, feldspar and clay minerals. Al_2O_3 and K_2O content can be related to the presence of potassium feldspars (microcline), mica and clay minerals. The Na_2O content is mainly related to plagioclase feldspar (albite). TiO_2 content principally relate to rutile and opaque minerals. Higher Fe_2O_3 may be related to the presence of iron oxide, heavy minerals or hematite cements. MgO content is related to the abundance of dolomite as grains or cements. CaO content is mostly related to the presence of calcite cements or skeletal fragments. CaO and MgO are mostly derived from carbonate grains and there is a strong positive correlation between CaO and MgO with loss on ignition (LOI) (Fig. 5).

The negative correlation of SiO_2 with most major elements (for example with Al_2O_3, Fig. 6) is due to most silica being sequestered in quartz, as indicated by Osman (1996). The high K_2O/Na_2O ratios are due to the presence

Table 1 Major and trace element contents in the sandstones of Sardar Formation

Sample No. (wt%)	SiO_2	Al_2O_3	Na_2O	MgO	K_2O	TiO_2	MnO	CaO	P_2O_5	Fe_2O_3	LOI
SH.23	94.38	2.34	0.06	0.01	0.14	0.16	0	0.81	0.04	1.02	0.92
SH.33	88.62	3.44	0.24	0	0.12	0.1	0.09	0.71	0.09	3.18	2.7
SH.39	77.09	6.21	0.05	0.23	0.76	0.45	0.03	6.3	0.04	3.15	5.45
SH.50	85.76	7.86	0.08	0.06	2.12	0.4	0	0.1	0.03	2.05	1.35
SH.52	87.16	7.84	0.03	0.09	0.78	0.38	0	0.21	0.05	1.37	1.84
SH.54	87.61	1.39	0.02	0.62	0.06	0.15	0.03	4.3	0.03	2.08	3.6
SH.88	79.33	13.03	0.04	0.26	1.87	0.47	0	0.34	0.04	1.93	2.53
SH.90	90.96	6.28	0.05	0.02	0.3	0.13	0	0.31	0.02	0.6	1.24
SH.95	72.73	9.25	0.03	0.89	1.36	0.31	0.06	5.39	0.05	3	6.81
SH.100	75.42	5.79	0.15	0.16	0.83	0.24	0.07	8.51	0.03	2.74	5.88
SH.113	90.84	1.65	0.01	0.01	0.44	0.07	0.02	2.21	0.03	2.71	1.96
SH.125	74.82	9.5	0.04	0.73	2.05	0.42	0.04	4.18	0.07	2.48	5.52
SH.146	97.74	0.66	0.03	0.01	0.03	0.04	0	0.41	0.02	0.75	0.25
SH.151	93.52	4.47	0.11	0.01	0.09	0.23	0	0.03	0.02	0.57	0.82
SH.153	98.06	0.61	0.04	0.01	0.06	0.39	0	0.01	0.05	0.49	0.06
SN.3	73.01	10.11	1.2	0.63	1.23	17.236	0.07	3.35	0.05	4.86	4.74
SN.16	80.87	11.03	1.19	0.38	1.7	0.48	0	0.34	0.06	1.89	1.88
SN.30	78	12.88	0.91	0.41	2.49	0.64	0	0.32	0.04	1.68	2.41
SN.39	92.4	4.41	0.32	0.08	1.04	0.21	0	0.07	0.01	0.97	0.38
SN.41	95.03	1.04	0.26	0.01	0.13	0.09	0.01	1.39	0.01	0.99	0.98
SN.45	96.78	1.25	0.06	0.01	0.21	0.07	0	0.09	0.01	1.4	0.06
SN.62	72.57	14.29	1.53	0.98	1.86	0.67	0.01	0.82	0.06	3.85	3.18
SN.82	81.45	6.93	0.71	0.3	1.28	0.42	0.06	3.21	0.04	2.29	3.15
SN.85	90.14	5.09	0.53	0.15	0.96	0.35	0.02	0.11	0.03	1.59	0.84
SN.95	82.46	10.5	1.28	0.2	1.6	0.54	0	0.21	0.03	1.29	1.69
SN.100	77.36	13.36	1.01	0.37	2.58	0.71	0	0.18	0.02	1.58	2.56
SN.108	88.07	4.05	0.36	0.14	0.95	0.22	0	0.01	0.02	2.69	2.2
SN.110	90.41	4.94	0.42	0.08	1.26	0.23	0	0.07	0.02	1.45	0.88
SN.115	96.36	1.82	0.1	0.01	0.31	0.1	0	0.03	0.02	0.82	0.31
SN.121	85.72	7.35	0.98	0.18	1.84	0.63	0	0.23	0.05	1.64	1.01

Note: LOI, loss of ignition

Table 1 Continued

Sample No. (ppm).	Co	Cr	Cu	Ni	U	Th	Sc	Ce	Pb	Rb	Sr	V	Y	Zr	Zn
SH.23	3	22	48	5	2	N	N	22	25	12	204	41	15	397	24
SH.33	78	11	35	59	7	11	1	20	63	7	432	40	17	338	87
SH39	19	74	56	11	5	14	2	31	52	51	247	88	25	1218	29
SH50	10	71	58	44	9	10	1	54	32	97	223	80	30	838	29
SH52	14	75	35	9	7	11	1	55	35	46	518	97	23	942	22
SH54	11	26	30	39	10	12	2	37	21	14	187	53	15	462	17
SH88	15	33	69	23	19	12	1	41	81	88	176	88	26	841	24
SH90	9	14	59	2	12	2	N	3	33	21	119	41	14	390	27
SH95	20	77	57	15	16	9	2	14	20	66	247	60	24	588	18
SH100	11	25	67	6	7	2	3	45	35	30	146	46	20	601	21
SH113	9	70	43	35	2	N	1	17	34	26	88	30	14	114	26
SH125	20	59	61	17	2	9	2	34	34	105	210	81	30	777	46
SH146	12	50	54	12	9	2	N	22	38	10	169	21	13	125	27
SH151	6	29	10	9	12	8	N	40	32	8	133	44	17	724	22
SH153	8	23	37	20	11	9	0	76	28	18	376	62	24	1238	34
SN.3	29	59	38	39	10	17	4	100	85	87	187	108	36	868	142
SN.16	12	57	66	4	8	11	1	50	36	113	157	90	32	924	41
SN.30	14	85	36	N	10	18	2	89	59	135	422	116	38	908	30
SN.39	16	53	48	N	N	N	0	53	20	65	97	40	19	551	22
SN.41	3	10	45	4	13	8	N	22	16	12	42	31	15	221	20
SN.45	11	101	43	N	4	4	0	44	26	24	50	26	13	165	19
SN.62	20	87	45	58	6	9	3	58	59	133	216	140	39	771	135
SN.82	15	32	31	23	9	18	2	59	47	71	118	73	28	1042	22
SN.85	9	52	40	19	13	8	4	60	41	65	101	69	27	1241	41
SN.95	17	48	44	11	12	23	0	53	43	100	220	89	33	1014	39
SN.100	7	67	51	12	14	13	2	83	67	155	170	125	45	1113	19
SN.108	21	59	72	N	2	6	2	52	117	46	88	49	22	507	29
SN.110	16	59	50	7	13	12	N	33	56	73	98	49	20	570	28
SN.115	13	25	22	N	11	10	0	15	46	29	150	32	12	176	17
SN.121	9	58	64	9	8	23	1	123	46	104	219	106	38	2207	27

Note: N=not detected, SH, Howz-e-Dorah section, SN, Niaz section.

of k-bearing minerals such as k-feldspar, mica (muscovite and biotite) and illite (Zhang, 2004; Osae et al., 2006). In these samples, TiO_2 concentration increases along with Al_2O_3 (Fig. 6), suggesting that TiO_2 is possibly associated with phyllosilicates minerals especially with illite (Dabard, 1990). According to the chemical composition diagram of Pettijohn (1975), sandstones are classified mainly as quartarenite, sublitharenite and subarkose (Fig. 7). This

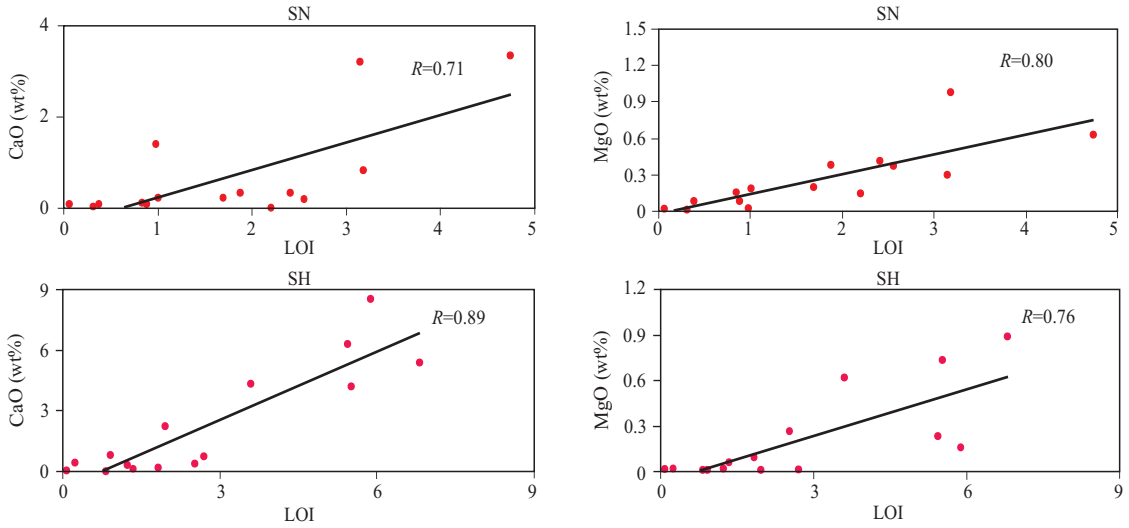

Fig. 5. Bivariate variation diagram for CaO, MgO and loss on ignition (LOI). (SN, Niaz section; SH, Howz-e-Dorah section).

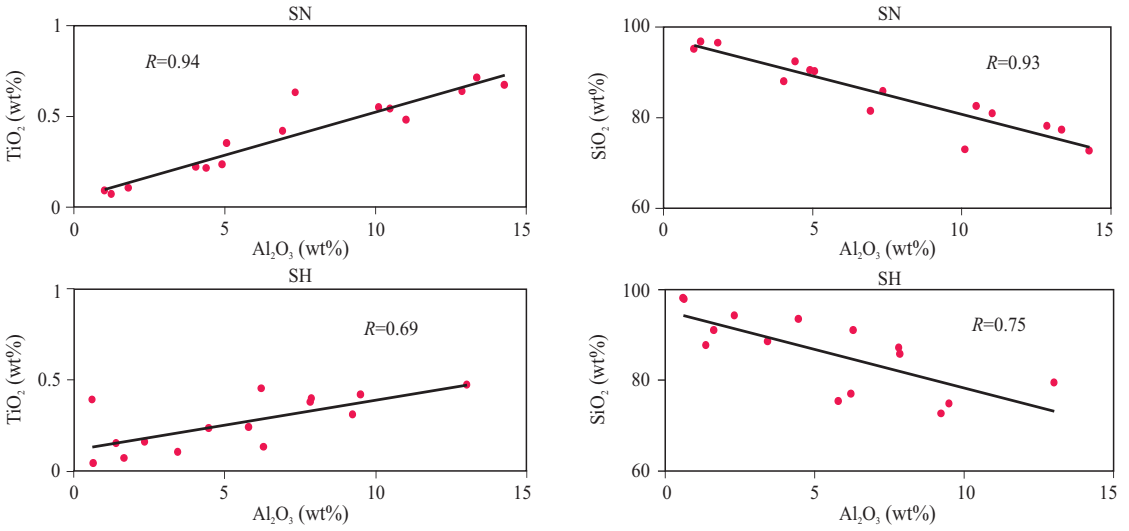

Fig. 6. The negative correlation between SiO_2 and Al_2O_3 and the positive correlation between TiO_2 with Al_2O_3. (SN, Niaz section; SH, Howz-e-Dorah section).

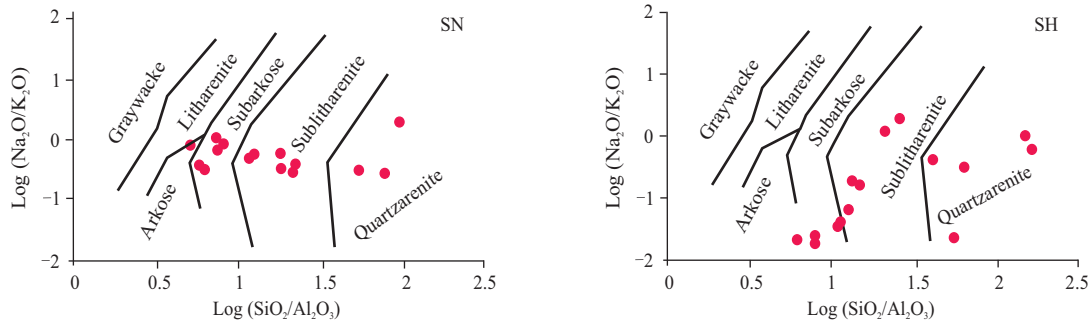

Fig. 7. Chemical composition of sandstones plotted on Pettijohn scheme (after Pettijohn, 1975) (SN, Niaz section; SH, Howz-e-Dorah section).

classification is generally consistent with the petrographic data. A positive correlation between Al_2O_3 and K_2O (Fig. 8) show that the concentration of the k-bearing minerals have significant effects on Al distribution that is controlled by the content of clay minerals (McLennan et al., 1983; Jin et al., 2006).

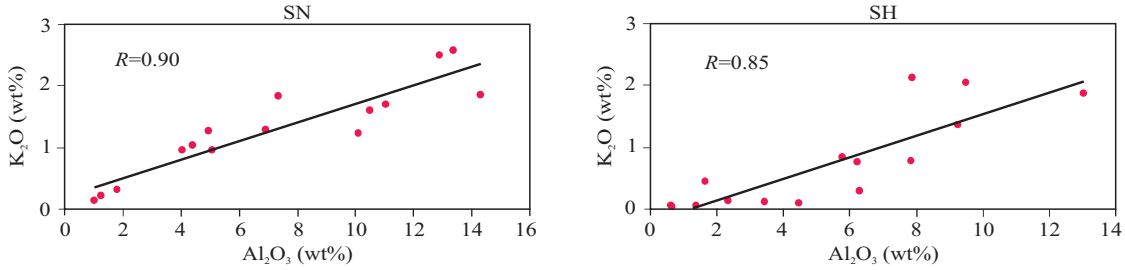

Fig. 8. Positive correlation Al_2O_3 versus K_2O (SN, Niaz section; SH, Howz-e-Dorah section).

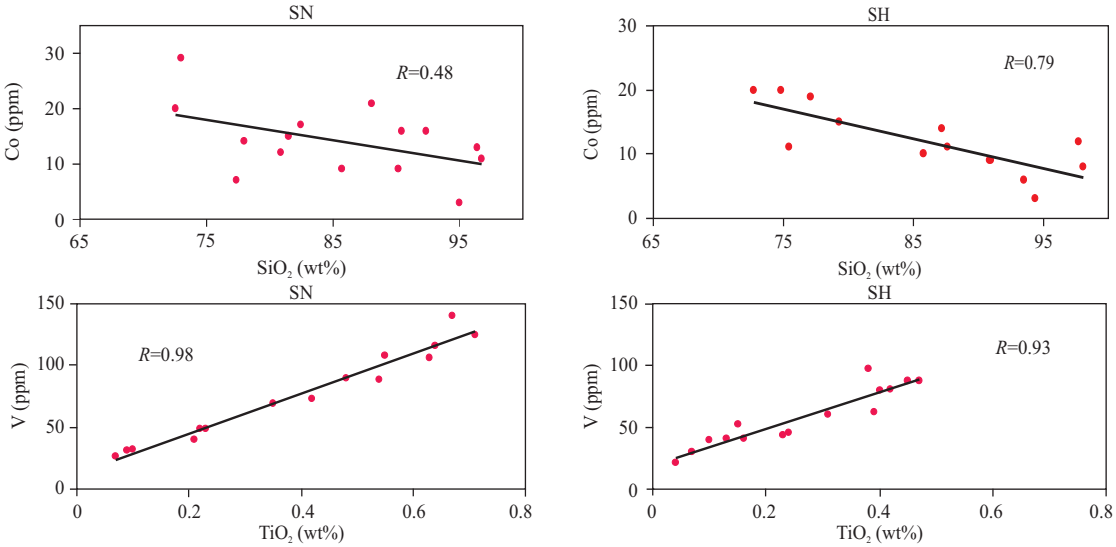

Fig. 9. Negative correlation of SiO_2 versus Co and positive correlation between TiO_2 and V (SN, Niaz section; SH, Howz-e-Dorah section).

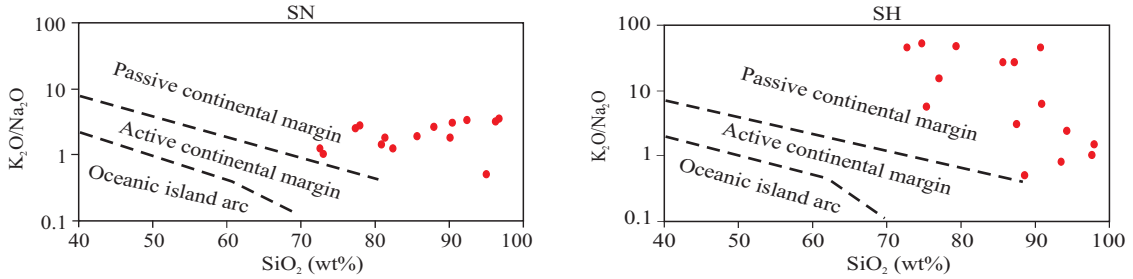

Fig. 10. Tectonic setting diagram for Sandstones of Sardar Formation (after Roser and Korsch, 1986) (SN, Niaz section; SH, Howz-e-Dorah section).

4.2.2 Trace elements

Table 1 shows selected trace and rare elements of the studied sandstone. The negative correlation between SiO_2 with the trace elements (Fig. 9) suggests that most of the trace elements are concentrated in the clay fraction (Akarish and El-gohary, 2008). These sandstones show enriched values of Zr, Sr and Rb and depletion in Nb, Y, Cr, Ni, Mo and Nd. Acidic or felsic rocks commonly have lower Y and Nb than basic rocks (Humphreys et al., 1995). This suggests that almost all of these sandstones were derived from plutonic and intermediate igneous terrains. High Zr contents in thin sections reflect that zirconium was released from plutonic rocks. On the other hand, the high values of Rb, Zr, Sr and low values of Cr and Ni suggest more felsic contribution than mafic to the Carboniferous sedimentary basin (Odigi and Amajor, 2009). Vanadium is positively correlated with TiO_2 (Fig. 9) and it is probably adsorbed on kaolinite or associated with iron oxide minerals (cf. Hirst, 1962; Abdel Wahab et al., 1997).

4.3 Provenance and tectonic setting

Several classifications have been proposed to discriminate from various origins and tectonic setting (Maynard et al., 1982; Bhatia, 1983; Bhatia and crook, 1986; Roser and Korsch, 1986, 1988). Roser and Korsch (1986) established a discrimination diagram using Log

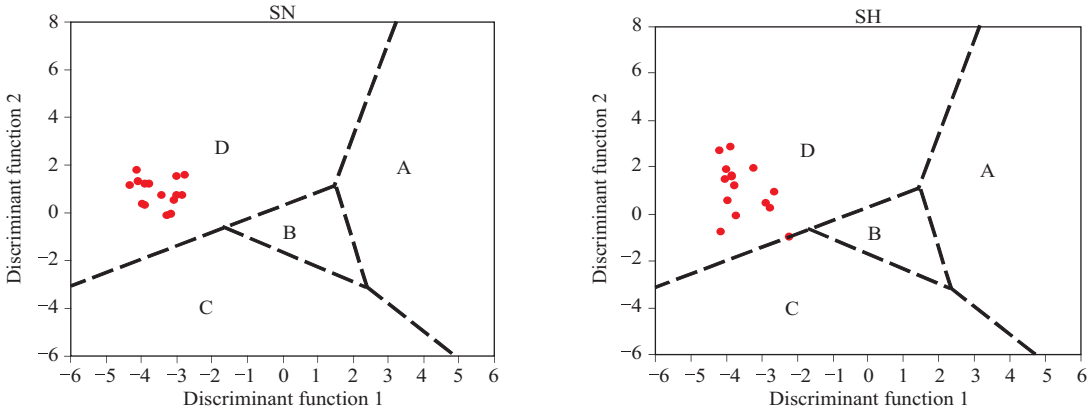

Fig. 11. Discrimination function plot of the sandstones of Sardar Formation (after Bhatia, 1983) (SN, Niaz section; SH, Howz-e-Dorah section), (A: Oceanic island arc, B: Continental island arc, C: Active continental margins and D: Passive margins)

Discriminant Function 1:

$-0.447SiO_2-0.972TiO_2+0.008Al_2O_3-0.267Fe_2O_3+0.208FeO-3.082MnO+0.140MgO+0.195CaO+0.719Na_2O-0.032K_2O+7.510P_2O_5+0.303$

Discriminant Function 2:

$-0.421SiO_2+1.988TiO_2-0.526Al_2O_3-0.551Fe_2O_3-1.610FeO+2.720MnO+0.881MgO-0.907CaO-0.177Na_2O-1.840K_2O+7.244P_2O_5+43.57$

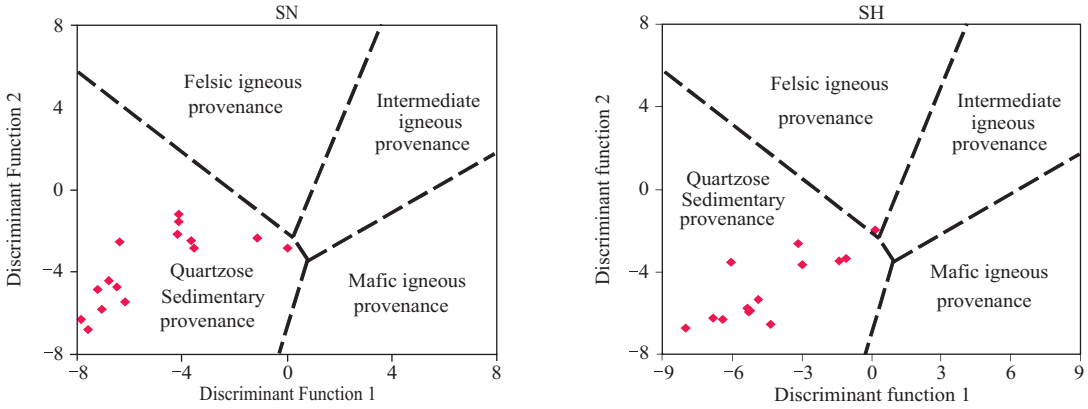

Fig. 12. Discriminnant plot for sandstones of Sardar Formation (after Roser and Korsch, 1988) (SN, Niaz section; SH, Howz-e-Dorah section)

Discriminant Function 1: $-1.733TiO_2+0.607Al_2O_3+0.76Fe_2O_3$ (t)$-1.5MgO+0.616CaO+0.509Na_2O-1.224K_2O-9.09$

Discriminant Function 2: $0.445TiO_2+0.07Al_2O_3-0.25Fe_2O_3$ (t)$-1.142MgO+0.438CaO+1.475Na_2O+1.426K_2O-6.861$

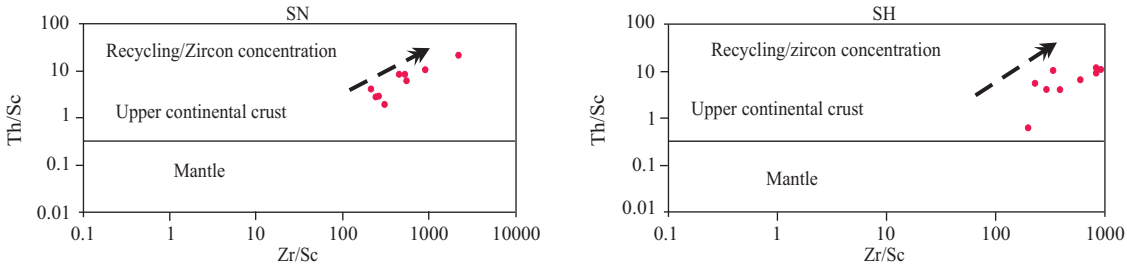

Fig. 13. Plot of Zr/Sc versus Th/Sc for sandstones of Sardar Formation (after McLennan et al., 1983) (SN, Niaz section; SH, Howz-e-Dorah section).

(K_2O/Na_2O) versus SiO_2 (Fig. 10) to determine the tectonic setting of terrigenous sedimentary rocks. In this diagram, the tectonic setting moves from the passive continental margin to the island arc with the decrease of SiO_2 content. Based on geochemical analysis, the Carboniferous sandstones plotted on the PM setting of Roser and Korsch (1986) diagrams.

The most important clues for the tectonic setting of the basin come from the relative depletion in oxides like CaO, Na_2O (the most mobile phases) and enrichment of SiO_2, TiO_2, etc. (the most immobile phases). The ratio of the most immobile to mobile oxides increases toward the PM tectonic setting due to the relative tectonic stability and hence protected weathering and high degree of recycling of sediments (Bhatia, 1983; Roser and Korsch, 1988). The samples of sandstones of Sardar Formation with multi-

variable major elements (11 oxides; Bhatia, 1983), are also plotted in passive continental margin setting (Fig. 11). Discriminant function analysis using major element compositions is another method for the sources of sandstones (Roser and Korsch, 1988). The discriminant functions of Roser and Korsch (1988) were designed to discriminate between four sedimentary provenance fields. This diagram (Fig. 12), suggests that the sediments may be derived from mature polycyclic continental sedimentary rock (quartzose sedimentary provenance). It also shows that they were derived from granitic-gneissic or sedimentary source area, similar to PM-derived (Roser and Korsch, 1988).

A number of heavy minerals (especially zircon) are dominated by trace elements, and thus their accumulation in high concentration may significantly influence trace element concentration in sandstones (McLennan et al., 1993). Zircon is present in the sandstone of Sardar Formation. The zircon enrichment in sandstones can be reflected by relationships between Zr/Sc and Th/Sc and the sedimentary sorting and recycling can also be monitored by a plot of Zr/Sc versus Th/Sc (McLennan et al., 1983). First-order sediments show a simple positive correlation between these ratios (i.e., Th/Sc and Zr/Sc), whereas recycled sediment shows a substantial increase in Zr/Sc with far less increase in Th/Sc. On this diagram, the analyzed samples are falling in the high Zr/Sc range typical of zircon concentration associated with sediment recycling and sorting (Fig. 13). The high values of Zr suggest more felsic contribution than mafic source rocks. Immobile elements like Zr, etc. are enriched in the PM setting (e.g. Bhatia, 1983). These sandstones are enriched in zircon, due to sedimentary sorting and recycling from pre-existing sandstones.

4.4 Weathering in the source area

The Chemical Index of Alteration (CIA) gives an indication of the degree of weathering in the source region (Nesbitt and Young, 1982). The CIA index is calculated using the equation:

$$CIA = \{Al_2O_3/(Al_2O_3+CaO^*+Na_2O+K_2O)\}\times 100$$

Values are expressed as molar proportions and CaO^* represents the CaO content of silicate minerals only (Fedo et al., 1995). Nesbitt and Young (1982) suggested a CIA value of nearly 100 for kaolinite and chlorite, and 70–75 for average shale. CIA values for fresh granite are around 50 (Visser and Young, 1990). High values indicate intensive chemical weathering in the source area while low rates (i.e., 50 or less) indicate unweathered source areas. CIA values for the Sardar sandstones vary from 36 to 80, with an average 71.65 for the Niaz section and from 24 to 95, with an average 66 for the Howz-e-Dorah section, indicating that the Sardar sandstones were derived from moderate to relatively high chemically weathered rocks in the source areas and during transportation before deposition. This could be due to humid climatic condition that promoted intense weathering. Plots of SiO_2 percentage versus total percent of $Al_2O_3+K_2O+Na_2O$, proposed by Suttner and Dutta (1986) was used in order to identify the chemical maturity of sandstones as a function of climate. This plot indicated the humid to sub-humid climatic conditions with high maturity for the studied samples (Fig. 14).

4.5 Carboniferous of East Central Iran in relation to Paleotethys Passive Margin

The results of our study can be correlated with paleomagnetic and paleotectonic maps of the Carboniferous period of the world (Golonka, 2007). A robust agreement of paleomagnetic poles of Iran and West Gondwana is observed for the Carboniferous, indicating that Iran was part of Gondwana during this time (Muttoni et al., 2009). During Carboniferous, an Iranian plate was located at 30°S (sub-tropical to tropical climate). In this paleo-tropical succession, humid to semi-humid climate

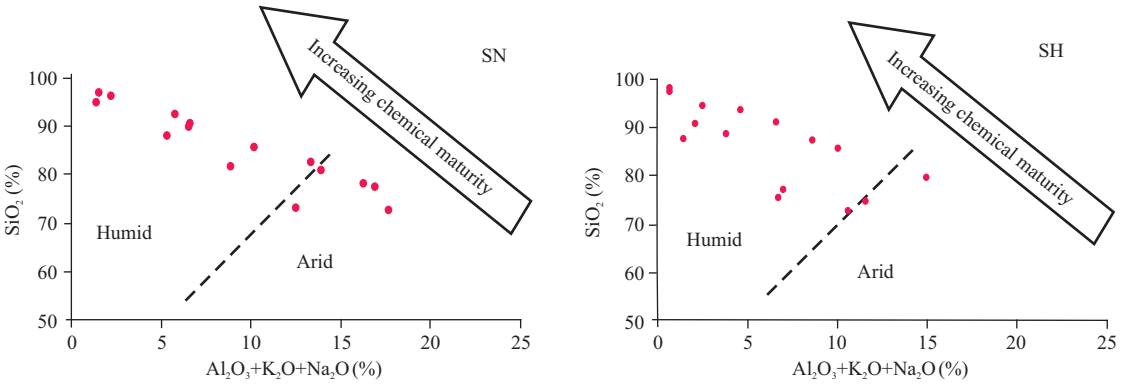

Fig. 14. Chemical maturity of the Sardar sandstones by bivariant plot of SiO_2 versus total $Al_2O_3+K_2O+Na_2O$. Fields after Suttner and Dutta (1986)
(SN, Niaz section; SH, Howz-e-Dorah section).

prevailed during the deposition of these sandstones. This can be supported by high quartz and low Al_2O_3 content (Fig. 14) in our analyzed samples as well as high CIA values, which are usually related to high weathering in more humid type climates. The elongate north-south trending trough in Tabas Block, a part of the Cimmerian Continent, is located between the Lut Block in the east and the Kalmard Block in the west, was suggested by Lasemi (1999, 2001) to have been a failed rift basin during the Late Paleozoic to Early Mesozoic times. Continued tectonic activity along the Nayband and Kalmard-Kuhbanan faults during Paleotethys rifting (Early Ordovician-Silurian) resulted in repeated vertical movement and formation of the Tabas failed rift basin (Lasemi, 1999, 2001). In the Tabas Block, the Ordovician-Silurian continental to shallow marine succession (the Shirgesht and Niur Formations) in the south changes to more than 1500 m of mainly deep marine siliciclastic turbidities to the north. This shows an overall transgression that can be related to the syn-rift phase of the Paleotethys margin (Lasemi, 2001). The sedimentary succession of the Tabas Block, like other parts of the Cimmerian Plates of central and northern Iran, consists of the Cambrian platform facies (pre-rift), Ordovician to Silurian siliciclastics and carbonates including basaltic flows (syn-rift) and the Devonian-Upper Triassic platform deposits (post-rift) can be related to the Paleotethys passive margin (Stampfli et al. 1991; Lasemi 1999, 2001). Petrography and geochemical data indicated that the sandstones of Sardar Formation (Carboniferous) in the Tabas Basin can have a source from the same tectonic settings and the Iranian plate was probably positioned on the north-facing passive margin of Gondwana. Our interpretation can further be supported by high quartz grain as well as high Zr/Sc and Th/Sc content in these sandstones.

5 Conclusions

Sardar Formation consists of sandstones, shales and limestones. The provenance of siliciclastic sediments of this formation has been interpreted by geochemical methods. The Sardar Sandstones of east-central Iran are probably enriched in quartz and poor in feldspar and lithic fragments and can be classified as quartzarenites, sublitharenites and subarkoses. They are cemented by silica, calcite, dolomite and hematite. Sandstones in the two lithostratigraphic sections have similar chemical composition from a common provenance. The dominance of quartz together with enrichment in the immobile elements such as Zr and Th, suggest that the tectonic setting of the depositional basin formed as part of a cratonic or passive margin setting. In these sandstones, Al_2O_3 and SiO_2 are commonly well negative correlated. The geochemistry of sandstones indicate that the tectonic setting of the study area were passive margin field. On the basis of the discrimination plots, the source sediments of the Sardar formation were polycyclic continental sedimentary rocks. The provenance of the studied samples was possibly rich in quartz as the presence of pre-existing sandstones (for example, Shirgesht Formation with age of Ordovician). High elemental ratios such as Zr/Sc and Th/Sc indicate a felsic and recycled source for the sandstones of Sardar Formation. The chemical results also show recycling of the sediments. Based on geochemical data, a climatic condition during the deposition of these sandstones was probably humid to sub-humid.

Acknowledgments

This study was supported by a grant to the senior author from Faculty of Sciences, Ferdowsi University of Mashhad. We also thank the Geology Department of Ferdowsi University of Mashhad for their logistic support during this study. We would like to acknowledge to Dr Fei Hongcai, editor of *Acta Geologica Sinica* (English Edition), and the two anonymous reviewers for their review and suggestions that improved our manuscript significantly.

Manuscript received Oct. 8, 2011
accepted Apr. 19, 2012
edited by Fei Hongcai

References

Abdel Wahab, H.Sh., Yemane, K., and Giegengack, R., 1997. Mineralogy and geochemistry of the Pleistocene lacusterine beds in Wadi Feiran, south Sinai, Egypt: Implication for environmental and climate changes. *Egyptian Journal Geology*, 41: 145–171.

Akarish, A.I.M., and El-Gohary, A.M., 2008. Petrography and geochemistry of lower Paleozoic sandstones, East Sinai, Egypt: Implication for provenance and tectonic setting. *Journal of African Earth Science*, 52: 43–54.

Alavi, M., 1996. Tectonostratigraphic synthesis and structural style of the Alborz Mountains System in northern Iran. *Journal of Geodynamics*, 11: 1–33.

Basu, A., Young, S.W., Suttner, L.J., James, W.C., and Mack, G. H., 1975. Re-evaluation of the use of undulatory extinction and polycrystallinity in detrital quartz for provenance interpretation. *Journal of Sedimentary Petrology*, 45: 873–882.

Bhatia, M.R., and Crook, K.A.W., 1986. Trace element characteristics of greywackes and tectonic discrimination of sedimentary basins. *Contribution to Mineralogy and Petrology*, 92: 181–193.

Bhatia, M.R., 1983. Plate tectonics and geochemical composition of sandstones. *Journal of Geology*, 91: 611–627.

Dabard, M.P., 1990. Lower Brioverian formations (Upper Proterozoic) of the Armorican Massif (France): Geodynamic

evolution of source areas revealed by sandstone petrography and geochemistry. *Sedimentary Geology*, 69: 45–58.

Dercourt, J., Ricou, L.E., and Vrielynck, B. (eds). 1993. *Atlas Tethys Paleoenvironmental Maps*. Gauthier-Villars, Paris, 307.

Dickinson, W.R., Beard, L.S., Brakenridge, G.R., Erjavec, J.L., Ferguson, R.C., Inman, K.F., Knepp, R.A., Lindberg, F.A., and Ryberg, P.T., 1983. Provenance of North American Phanerozoic sandstones in relation to tectonic setting. *Geological Society of America Bulletin*, 94: 222–235.

Dickinson, W.R., 1985. Interpreting provenance relations from detrital modes of sandstones. In: Zuffa, G.G. (Eed.), *Provenance of Arenites*. Reidel, Dordrecht, 333–361.

Fedo, C.M., Nesbitt, H.W., and Young, G.M., 1995. Unraveling the effect of potassium metasomatism in sedimentary rocks and paleosols, with implication for paleoweathring conditions and provenance, *Geology*, 23: 921–924.

Golonka, J., 2007. Phanerozoic paleoenvironment and paleolithofacies maps, Late Paleozoic. *Geologia*, 33: 145–209.

Hirst, D.M., 1962. The geochemistry of modern sediments from the Gulf of Paria. II. The location and distribution of trace elements. *Geochimica et Cosmochimica Acta*, 26: 1174–1187.

Humphreys B., Morton A.C., Hallsworth C.R., Gatliff W.R., and Riding J., 1995. An integrated approach to provenance studies: A case example from the Upper Jurassic of the Central Graben, North Sea. In: Morton, A.C., Todd, S.P., and Haughton, P.D. W. (eds), *Developments in Sedimentary Provenance Studies*, 230–251. Published by the Geological Soc. London.

Jin, Z., Li, F., Cao, J., Wang, S., and Yu, J., 2006. Geochemistry of Daihai Lake sediments, Inner Mongolia, north China: Implications for provenance, sedimentary sorting and catchment weathering. *Geomorphology*, 80: 147–163.

Lasemi, Y., 1999. *Depositional environments of the Ordovician rocks of Iran (syn-rift sequence) and formation of the Paleotethys passive margin*. Proceedings of the 17th annual meeting of the Geological Survey of Iran, 158–160 (in Persian).

Lasemi, Y., 2001. *Facies Analysis, depositional environments and sequence stratigraphy of the upper Pre-Cambrian and Paleozoic rocks of Iran*: Geological Survey of Iran, 180 (in Persian).

Lasemi, Y., Ghomashi, M., Amin-Rasouli, H., and Kheradmand, A., 2008. The lower Triassic Sorkh Shale Formatin of the Tabas Block, East Central Iran: Succession of failed-rift at the Paleotethys margin. *Carbonate and Evaporites*, 23(1): 21–38.

Maynard, J.B., Valloni, R., and Yu, H.S., 1982. Composition of modern deep-sea sands from arc-related basins. Trench-Forearc Geology: Sedimentation and tectonics on modern and ancient active plate margin. *Geological Society of London, Special Publications*, 551–561.

McLennan, S.M., Taylor, S.R., and Eriksson, K.A., 1983. Geochemistry of Archean shales from the Pilbara Supergroup, Western Australia. *Geochimica et Cosmochimica Acta*, 47: 1211–1222.

Muttoni, G., Mattei, M., Balini, M., Zanchi, A., Gaetani, M., and Berra. F., 2009. The drift history of Iran from the Ordovician to the Triassic, *Geological Society of London, Special Publications*, 312: 7–29.

Nesbitt, H.W., and Young, G.M., 1982. Early Proterozoic climates and plate motions inferred from major element chemistry of lutites. *Nature*, 299: 715–717.

Odigi, M.I., and Amajor, L.C., 2009. Geochemical characterization of Cretaceous sandstones from the Southern Benue Trough, Nigeria. *Chinese Journal of Geochemistry*, 28: 044–054.

Osae, S., Asiedu, D.K., Banoeng-Yakubo, B., Koeberl, C., and Dampare, S.B., 2006. Provenance and tectonic setting of late Proterozoic Buem sandstones of southeastern Ghana: Evidence from geochemistry and detrital modes. *Journal of African Earth Sciences*, 44: 85–96.

Osman, M., 1996. *Recent to Quaternary River Nile Sediments*: A sedimentological characterization on samples from Aswan to Naga-Hammadi, Egypt. Unpub. Ph.D. thesis, Univ. of Vienna, Vienna, 162.

Pettijohn, F.J., 1975. *Sedimentary rocks*, 3rd edition, New York: Harper and Row, 628.

Roser, B.P., and Korsch, R.J., 1986. Determination of tectonic setting of sandstone–mudstone suites determined using SiO_2 content and K_2O/Na_2O ratio. *Journal of Geology*, 94: 635–650.

Roser, B.P., and Korsch, R.J., 1988. Provenance signatures of sandstone-mudstone suites determined using discriminant function analysis of major-element data. *Chemical Geology*, 67: 119–139.

Scotese, C.R., and Langford, R.P., 1995. Pangea and the paleogeography of the Permian. In: Scholle, P.A., Peryt, Scholle, T.M., Peryt, and Ulmer-Scholle, D.S. (Ulmer-Scholle, eds.), *The Permian of Northern Pangea*, v. I. Berlin: Springer-Verlag, 3–19.

Sengor, A.M.C., 1984. The Cimmeride orogenic system and the tectonics of Eurasia. *Geological Society of America Special Paper* 195, 82.

Stampfli, G., Marcoux, J., and Baud, A., 1991. Tethyan margins in space and time. *Palaeogeography, Palaeoclimatology, and Palaeoecology,* 87: 373–409.

Stampfli, G., and Pillevuit, A., 1993. An alternative PermoTriassic reconstruction of the kinematics of the Teyhan realm. In: Dercourt, J., Ricou, L.E., and Vrielynck, B. (eds.), *Atlas Tethys Paleoenvironmental maps*. Paris. GauthirVillars, 55–62.

Suttner, L.J., and Dutta, P.K., 1986. Alluvial sandstone composition and paleoclimate, I. framework mineralogy. *Journal of Sedimentary Petrology*, 56: 329–345.

Visser, J.N.J., and Young, G.M., 1990. Major element geochemistry and paleoclimatogy of the Permo-Carboniferous glacigene Dwyka Formation and post-glacial mudrocks in southern Africa. *Palaeogeography, Palaeoclimatology, Palaeoecology*, 81: 49–57.

Zhang, K.L., 2004. Secular geochemical variations of the Lower Cretaceous siliciclastic from central Tibet (China) indicate a tectonic transition from continental collision to back-arc rifting. *Earth and Planetary Science Letters*, 229: 73–89.